ACS SENSORS

Article

Cite This: ACS Sens. XXXX, XXX, XXX−XXX

pubs.acs.org/acssensors

OLIVe: A Genetically Encoded Fluorescent Biosensor for Quantitative Imaging of Branched-Chain Amino Acid Levels inside Single Living Cells

Tomoki Yoshida, Hitomi Nakajima, Sena Takahashi, Akira Kakizuka, and Hiromi Imamura*

Department of Functional Biology, Graduate School of Biostudies, Kyoto University, Yoshida-konoe-cho, Sakyo-ku, Kyoto 606-8501, Japan

Supporting Information

ABSTRACT: Branched-chain amino acids (BCAAs) are essential amino acids, controlling cellular metabolic processes as signaling molecules; therefore, utilization of intracellular BCAAs may be regulated by the availability of nutrients in the environment. However, spatial and temporal regulation of intracellular BCAA concentration in response to environmental conditions has been unclear due to the lack of suitable methods for measuring BCAA concentrations inside single living cells. Here, we developed a Förster resonance energy transfer (FRET)-based genetically encoded biosensor for BCAAs, termed optical biosensor for leucine−isoleucine−valine (OLIVe). The biosensor showed approximately 2-fold changes in FRET values corresponding to BCAA concentrations. Importantly, FRET signals from HeLa cells expressing OLIVe in the cytoplasm and nucleus correlated with bulk intracellular BCAA concentrations determined from populations of cells by a biochemical method, and were decreased by knockdown of L-type amino acid transporter 1 (LAT1), a transporter for BCAAs, indicating that OLIVe can reliably report intracellular BCAA concentrations inside single living cells. We also succeeded in imaging BCAA concentrations in the mitochondria using mitochondria-targeted OLIVe. Using the BCAA imaging technique, we found apparently correlated concentrations between the cytoplasm and the mitochondria. We also found that extracellular non-BCAA amino acids affected intracellular BCAA concentrations. Of these amino acids, extracellular glutamine markedly increased intracellular BCAA concentrations in a LAT1-dependent manner. Unexpectedly, extracellular pyruvate was also found to have significant positive effects on maintaining intracellular BCAA concentrations, suggesting that the cells have pyruvate-dependent systems to import BCAAs and/or to regulate BCAA metabolism.

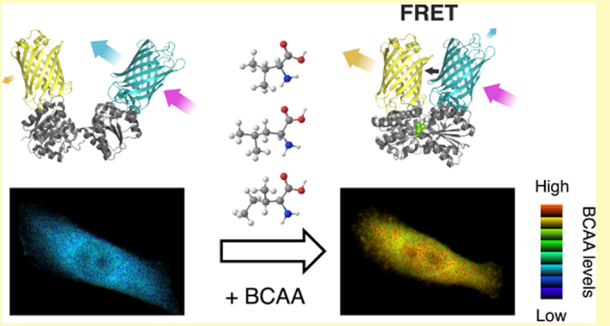

KEYWORDS: *BCAA, leucine, isoleucine, valine, biosensor, FRET, single cell, live imaging*

INTRODUCTION

Branched-chain amino acids (BCAAs), leucine, isoleucine, and valine, are essential amino acids for the synthesis of protein, as well as sources for the biosynthesis of ketone bodies, glucose, and nonessential amino acids, such as alanine, glutamate, and glutamine, in animals.[1,2] Previous pathological and physiological studies have reported alterations in blood BCAA levels in several illnesses and pathologies; liver disease,[3,4] chronic kidney disease,[5,6] chronic obstructive pulmonary disease,[7] urea cycle disorders,[8] and traumatic brain injury[9] have been linked to decreases in BCAA levels, while increased BCAA levels correlate with insulin resistance,[10] type 2 diabetes mellitus,[11,12] coronary artery disease,[13,14] maple syrup urine disease,[15] and obesity.[16] In addition, beneficial effects of supplementation or restriction of BCAAs have been suggested for several illnesses, including the diseases described above,[4,10,15,17−23] as well as for longevity in model organisms such as mouse,[24] fruit fly,[25] and nematode.[26] These facts highlight the potential significance of BCAA levels in regulating cellular functions.

Previously, measurements of BCAAs have been carried out using enzymatic spectrophotometry[27] or chromatographic techniques.[28−34] These methods are useful for determination of BCAA levels in extracts pooled from a large number of cells. However, the requirement of cell lysis makes it impossible to analyze the spatiotemporal dynamics of BCAA levels inside living cells. Consequently, this has hindered the elucidation of cellular mechanisms that control intracellular BCAA levels as well as the roles of BCAAs in regulating cellular processes.

Metabolite imaging using genetically encoded fluorescent biosensors is increasingly recognized as an important technique to reveal the spatiotemporal dynamics of metabolites inside living cells, the utility of which was clearly demonstrated for metabolites such as glucose,[35] glutamine,[36] adenosine 5′-triphosphate (ATP),[37] and NAD^+/NADH.[38,39]

Received: October 21, 2019
Accepted: December 5, 2019

DOI: 10.1021/acssensors.9b02067
ACS Sens. XXXX, XXX, XXX−XXX

In this study, we developed a genetically encoded Förster resonance energy transfer (FRET)-based biosensor that responds to leucine, isoleucine, and valine. The biosensor enabled quantitative imaging of the intracellular BCAA levels within the nucleocytoplasm or mitochondria of individual living mammalian cells, and revealed a complex regulation of intracellular BCAA levels in response to changes in the nutritional environment of the cells.

EXPERIMENTAL SECTION

Chemicals. *N*-(2-Hydroxyethyl)piperazine-*N*′-ethanesulfonic acid (HEPES) and 3-(*N*-morpholino)propanesulfonic acid (MOPS) were purchased from Dojindo Laboratories (Kumamoto, Japan). BCAA metabolites: sodium 3-methyl-2-oxobutyrate was obtained from Sigma-Aldrich; 4-methyl-2-oxovaleric acid and 3-methyl-2-oxovaleric acid were obtained from Tokyo Chemical Industry (Tokyo, Japan). Solutions of BCAA metabolites were neutralized with sodium hydroxide before use. Other chemicals were purchased from Nacalai Tesque (Kyoto, Japan) unless otherwise noted. All chemical reagents and other solvents used were analytical grade.

Cells and Cell Culture. HeLa cells were routinely cultured in Dulbecco's modified Eagle's medium (DMEM, 1 g/L glucose; Nacalai Tesque) with 10% fetal bovine serum (FBS; Sigma-Aldrich) at 37 °C, 5% CO_2. Cells expressing the biosensor were generated by transfection with plasmids carrying the biosensor complementary DNA (cDNA) using Lipofectamine 2000 reagent (Invitrogen) according to the manufacturer's instructions. Cells stably expressing the biosensor were isolated following a protocol described in a previous report.[40]

Gene Construction. A cDNA for optical biosensor for leucine−isoleucine−valine (OLIVe) was synthesized by Genscript. The OLIVe cDNA was inserted between XhoI and HindIII sites of pRSET-B and pcDNA3.1(−) vectors to produce pRSET-OLIVe and pcDNA-OLIVe, respectively. To generate pcDNA-mit-OLIVe, the OLIVe cDNA was further amplified by polymerase chain reaction (PCR), and inserted between BamHI and HindIII sites of a pcDNA-mit vector, which was prepared from pcDNA-mitATeam1.03 by digestion with BamHI and HindIII.[37] The constructs used in the present study are illustrated in Figure S1.

Purification of the Biosensor. For in vitro characterization, the protein was purified according to a protocol described in a previous report[41] with slight modifications. The protein was purified from the lysate of *Escherichia coli* strain JM109 (DE3) carrying the biosensor plasmid using a Ni−NTA Superflow column (QIAGEN). The protein was further purified on a Superdex 200 gel-filtration column (GE Healthcare) pre-equilibrated with 20 mM of Tris−HCl (pH 8.0) and 150 mM of sodium chloride. The purified protein was stored at 4 °C and used within 12 weeks of purification.

Characterization of the Biosensor in Vitro. Fluorescence spectra of the purified biosensor were measured using an FP-6500 spectrofluorometer (Jasco). After 1 h stabilization at 37 °C in 10 mM of phosphate-buffered saline (PBS) (pH 7.4, Wako) containing 10% sucrose, 1% bovine serum albumin (BSA), 0.1% NP-40, 50 mM of NaCl, and 100 μM of tris(2-carboxyethyl)phosphine (TCEP) (buffer A), fluorescence spectra from 460 to 600 nm were scanned at a scanning speed of 1000 nm/min. The excitation wavelength was 435 ± 2.5 nm. Sucrose and NP-40 were added to stabilize the diluted biosensor. The amino acid selectivity of OLIVe was investigated at 37 °C in buffer A containing 0.1−1 mM of each amino acid, respectively. The pH dependency of the biosensor was investigated at 37 °C with 0−10 mM of leucine in 50 mM of MOPS−KOH (pH 6.3−7.5) or HEPES−KOH (pH 7.7−8.3) containing 10% sucrose, 1% BSA, 0.1% NP-40, 50 mM of NaCl, and 100 μM of TCEP. The values of $K_{0.5}$ were calculated using Hill equations: $R = (R_{max} - R_{min}) \times [S]^n/([S]^n + K_{0.5}{}^n) + R_{min}$, where n is the Hill coefficient, and R_{max} and R_{min} are the maximum and minimum ratios of the 527/475 nm peak intensity, respectively. The purified protein, still containing a His-tag at the N-terminus, was used for in vitro characterization. The amino acid sequence of the His-tagged OLIVe is shown in Figure S1.

Note that the FRET signals were considerably perturbed by redox states in the measurement conditions, as displayed by their significant increases in the presence of an oxidant even without the addition of any amino acids (Figure S2). This may be due to conformational changes derived from a formation of a disulfide bond inside leucine/isoleucine/valine-binding protein (LIVBP).[42] Because it has been demonstrated that the cellular redox potential is maintained at a relatively low level (approximately −240 mV),[43] the disulfide bond should not form in the cytosol and mitochondria in living cells. Nevertheless, in the present study, in vitro characterizations of purified OLIVe were carried out in the presence of a reducing agent (100 μM TCEP).

High-Performance Liquid Chromatography (HPLC) Analysis of Free Amino Acid Concentrations in Cells. Cells were trypsinized and suspended in precooled PBS, followed by measuring cell number and cell volume in the suspension with a TC10 cell counter (Bio-Rad). To prepare samples for HPLC analysis, aliquots of the suspension were further collected by centrifugation at 6000*g* for 3 min at 4 °C. Pellets were disrupted by ultrasonication in 80% MeOH for 20 min at room temperature, followed by centrifugation at 13 000*g* for 15 min. Aliquots of the supernatant were filtered (pore size; 0.2 μm), and free amino acids in the samples were analyzed using an Agilent 1100 system equipped with an Agilent Poroshell 120 EC-C18 column (3.0 × 150 mm^2, 2.7 μm) according to the manufacturer's instructions. For labeling amino acids in samples, an *o*-phthaldialdehyde (OPA)/fluorenylmethyloxycarbonyl chloride (FMOC) derivatization method was used. Cellular concentrations of individual amino acids were calculated using the following equation: Cellular amino acid concentration = [amino acid]/(CN × CV), where [amino acid] and CN represent the total amino acid concentrations and total cell number in the aliquot, respectively, and CV represents the cell volume estimated from the diameters of the trypsinized cells.

Microscopy Assay. Fluorescent dual emission ratio imaging was carried out according to a previous report.[37] Prior to imaging, the culture medium was changed to phenol red-free DMEM containing 5% FBS without vitamin B_2, and the cells were incubated at 37 °C with 5% CO_2 for 5−10 h. Exclusion of phenol red and vitamin B_2 was performed to reduce autofluorescence from the medium during imaging. Imaging was performed on a Nikon Eclipse Ti-E inverted microscope with a perfect focus system (Nikon Instruments) using the following objective lenses (Nikon Instruments): a CFI Plan Apo 20× (NA; 0.75) for the images in Figures 2G and S4, a CFI Apo TIRF 60× (NA; 1.49) objective lens for Figures 2A and 3A, and a CFI Plan Apo λ 40× (NA; 0.95) for the rest of the imaging experiments. Fluorescence emissions were captured using a 400−600 ms exposure time using an sCMOS camera (Zyla4.2, Andor Technology) for Figure 2C,D and Supplemental Movie 1, or a charge-coupled device (CCD) camera (ORCA-AG, Hamamatsu Photonics) for the rest of the imaging experiments. The FRET signals were assessed by the ratio of yellow fluorescent protein (YFP)/cyan fluorescent protein (CFP) fluorescence emissions, which was calculated using the integrated intensity of YFP emission and CFP emission within the area of the whole cell for cytosol or the area surrounding the mitochondria for mitochondria inside individual cells, respectively. The following filter sets (Semrock) were used for the imaging: an FF01-427/10 excitation filter, an FF458-Di01 dichroic mirror, and two emission filters (FF01-483/32 for CFP and FF01-542/27 for YFP). The BCAA levels were converted to pseudo-color images generated by the emission ratio of YFP/CFP calculated from the YFP and CFP fluorescence images. Analysis of the images was performed using MetaMorph software (Molecular Devices). The background subtraction was carried out using a fluorescence signal within an area devoid of cells as a background signal.

Western Blot Analysis. Protein expression levels were investigated by western blotting analysis. The following primary antibodies were used: a rabbit polyclonal antibody against L-type amino acid transporter 1 (LAT1) (Cell Signaling, #5347, 1:1000 dilution ratio) and a mouse monoclonal antibody against actin (Merck, MAB1501, 1:2500 dilution ratio). Horseradish peroxidase (HRP)-labeled anti-mouse or -rabbit IgG antibodies (GE Healthcare, 1:2500 dilution

DOI: 10.1021/acssensors.9b02067
ACS Sens. XXXX, XXX, XXX−XXX

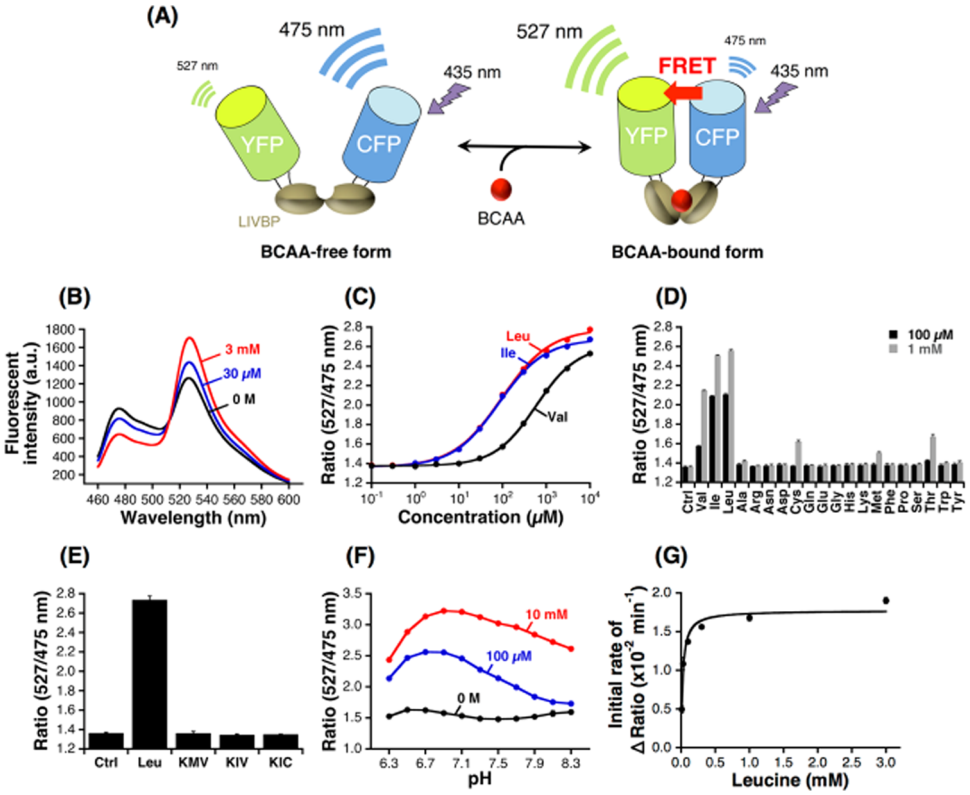

Figure 1. Characterization of a FRET-based BCAA biosensor, OLIVe. (A) Schematic model of the developed biosensor. In the absence of BCAAs, LIVBP adopts an opened form (BCAA-free form). Upon BCAA binding, its conformation changes, leading to a closed form (BCAA-bound form). Accompanied by these conformational changes, the distance between CFP and YFP inserted into LIVBP is altered, which translates to alterations in FRET efficiency from CFP to YFP. (B) Representative emission spectra changes with BCAAs in vitro. Fluorescence emission spectra of the biosensor at various leucine concentrations (0−10 mM) were examined at 37 °C. (C) Changes in the fluorescence emission ratio (527/475 nm) along with BCAA concentrations. The emission ratio values of the biosensor at 37 °C were plotted against BCAA concentrations. The regression model was obtained using Hill equations. (D, E) The selectivity of the biosensor among (D) amino acids (100 μM to 1 mM) and (E) BCAA metabolites (1 mM). KIV, KMV, and KIC represent α-ketoisovalerate, α-keto-methylvalerate, and α-ketoisocaproate, respectively. Ctrl: buffer without any amino acids. (F) pH dependency of the biosensor. (G) Representative initial rate changes in the emission ratio of the biosensor binding a BCAA. Rate changes in fluorescence emission spectra of the biosensor at various leucine concentrations (10 μM to 3 mM) were examined. For (B)−(G), the values represent mean ± SD (n = 3, independent repetitions).

ratio) were used as the secondary antibody. Chemi-Lumi One reagent (Nacalai Tesque) was used as the HRP substrate. An LAS4000 imager (GE Healthcare) was used to detect luminescence.

siRNA Treatment. The following predesigned and validated siRNA duplexes (Silencer Select siRNAs, Invitrogen) were used for suppressing the expression of human LAT1: s15653 for siLAT1#1 and s15655 for siLAT1#2. Negative control experiments were carried out using Silencer Select Negative Control #1 siRNA (Invitrogen). Lipofectamine RNAiMAX reagent (Invitrogen) was used for transfection of siRNAs according to the manufacturer's protocol.

siRNA#1
Sense: 5′-UGUCCAAUCUAGAUCCCAAtt-3′
Antisense: 5′-UUGGGAUCUAGAUUGGACAca-3′
siRNA#2
Sense: 5′-ACAGAAAGCCUCACUUCAtt-3′
Antisense: 5′-UCAAGCUCAGGCUUUCUGUgg-3′

RESULTS AND DISCUSSION

Development and Characterization of a FRET-Based BCAA Biosensor. A FRET-based BCAA biosensor, termed optical biosensor for leucine−isoleucine−valine (OLIVe), was developed by combining the gene for leucine/isoleucine/valine-binding protein (LIVBP) from *E. coli* with seCFP (a variant of cyan fluorescent protein, CFP)[44] and cp173-Venus (a variant of yellow fluorescent protein, YFP)[45] as a donor and an acceptor, respectively. LIVBP belongs to the bacterial periplasmic binding protein superfamily. Periplasmic binding proteins, or substrate-binding proteins, for a wide variety of ligands have been identified, including ions, heme, carbohydrates, and amino acids.[46,47] Commonly, these proteins have a ligand-binding site at the interface of two domains, and undergo a large conformational change upon ligand binding. These features make periplasmic binding proteins attractive materials for biosensors,[46] and in fact, Frommer and coworkers have succeeded in developing a series of genetically encoded fluorescent biosensors for metabolites, including glucose, maltose, and glutamine, by fusing fluorescent proteins to periplasmic binding proteins.[35,36,48] However, a previous crystallographic study of LIVBP revealed that in spite of the large global conformational changes, binding of BCAA leaves the distance between the N- and C-termini of the protein virtually unaltered (from 48.5 to 51.5 Å) (PDB accession codes: 1z15 and 1z16).[49] Thus, the simple fusion of fluorescent proteins to the N-terminal and C-terminal ends of the protein was expected to result in poor FRET gain upon ligand binding. In fact, the ligand-induced FRET gain of recently reported fluorescent biosensors for leucine (FLIP-Leu), in which CFP and YFP are fused to the N- and C-termini of periplasmic leucine-binding protein (LBP), respectively, is quite small.[50] LIVBP and LBP share ≈80% amino acid

DOI: 10.1021/acssensors.9b02067
ACS Sens. XXXX, XXX, XXX−XXX

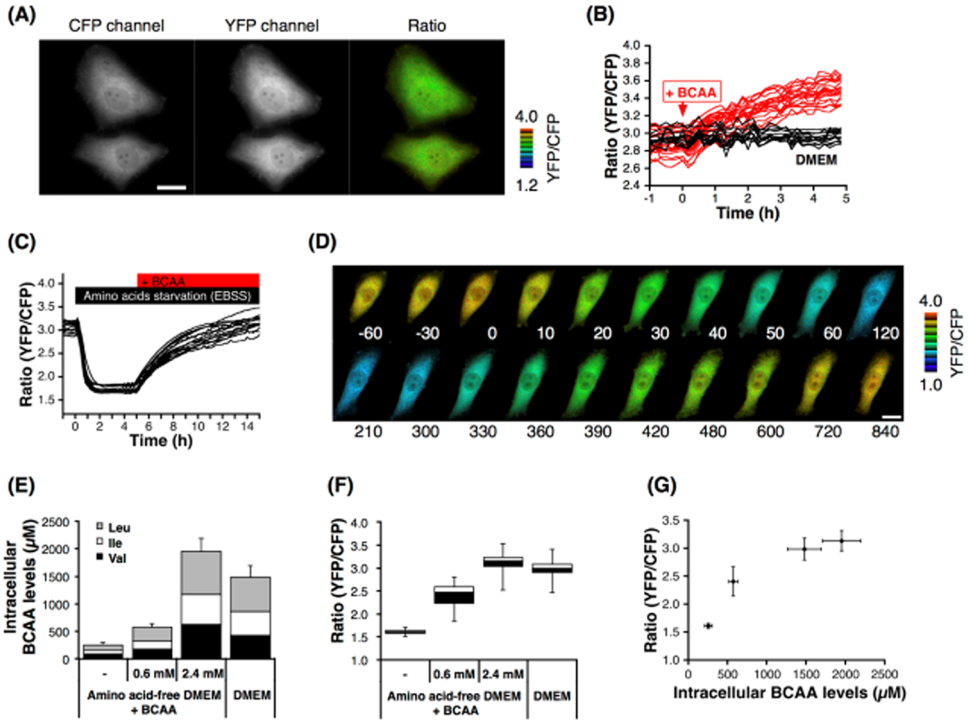

Figure 2. Monitoring of intracellular BCAA levels in HeLa cells. (A) Representative wide-field images of CFP (left), YFP (middle), and FRET signals (right) of a single OLIVe-expressing HeLa cell. Images of FRET signals are presented in pseudo-color corresponding to the values of the YFP/CFP emission ratio. Scale bar represents 20 μm. (B, C) Representative time course of FRET signals of OLIVe-expressing cells in various culture conditions. For (B), cells were cultured in normal culture medium (DMEM) (black line) or DMEM containing excess (24 mM) BCAA (red line). At time = 0, DMEM or BCAA solution was added. For (C), cells were treated with amino acid-free medium [Earle's balanced salt solution (EBSS)] at time = 0 (h). Subsequently, 2.4 mM of BCAA (equivalent to the BCAA amounts in DMEM) were added to the EBSS at time = 5 (h). Each line represents FRET signals of individual cells. For (B), and (C), three independent experiments gave consistent results. (D) Representative sequential wide-field images of FRET signals of a single cell, corresponding to the results in (C). The values below the images represent time (min) after the EBSS treatment. Scale bar represents 20 μm. (E) Intracellular BCAA concentrations estimated by HPLC. (F) Distribution of FRET signals of single OLIVe-expressing cells. After a 6-h incubation in media with various BCAA concentrations, cells were subjected to measurements of BCAAs with (E) an HPLC technique [n = duplicate or triplicate; the values represent mean ± standard deviation (SD)] or (F) an imaging system using the biosensor. For (E), box-and-whisker plots of values in FRET signals from individual cells are shown (n = 54−63 cells for each treatment, from three independent repetitions). (G) Correlation between bulk intracellular BCAA concentrations and the average values of the FRET signals. The total values of each BCAA concentration determined by HPLC vs the average values of FRET signals were plotted. The values represent mean ± SD. The data were corresponding to the assays (E, F).

identities, and the distance between N- and C-termini of LBP is, like LIVBP, almost unchanged upon ligand binding. In contrast to the distance between N- and C-termini, the distance between amino acid positions 180 and 270 in LIVBP is reduced from 46.0 to 30.9 Å upon BCAA binding. We thus inserted YFP between amino acid positions 180 and 181, and CFP between amino acid positions 269 and 271 of LIVBP, with short glycine-based linkers (Figures 1A and S1), rather than simply fusing the fluorescent proteins to both ends of the protein; in principle, this should yield a larger FRET gain.[51]

When the purified biosensor was excited at 435 nm, two fluorescent emission peaks were detected at 475 and 527 nm, derived from CFP and YFP, respectively (Figure 1A,B). The emission spectrum of the biosensor changed depending on the BCAA concentration, where an increase in the BCAA concentration and YFP intensity was inversely correlated with CFP intensity (Figure 1B). Based on this property, FRET signals from the biosensor can be assessed by the emission ratios of YFP/CFP, and reflect BCAA concentrations (Figure 1C). The dynamic range of FRET signals was approximately 105%, as displayed by the maximum increment in FRET signals in the presence of 10 mM of leucine (Figure 1C). The affinity of the biosensor for BCAAs ($K_{0.5}$) was 97 ± 3, 83 ± 1, and 589 ± 23 μM for leucine, isoleucine, and valine, respectively. These values are higher than those previously reported for the original LIVBP (8 μM for leucine).[41] The disparities might be due to the insertion of the fluorescent proteins into LIVBP, which could affect the conformation of LIVBP. We examined the selectivity of the biosensor for all 20 individual amino acids (0.1−1 mM), and found that significant increases in the FRET signals were observed only in the presence of leucine, isoleucine, or valine (Figure 1D). We did observe slight increases in the FRET signals at relatively high concentrations of cysteine, methionine, or threonine. The metabolites of BCAA, their corresponding α-ketoacids [α-ketoisovalerate (KIV) for valine, α-keto-methylvalerate (KMV) for isoleucine, α-ketoisocaproate (KIC) for leucine], did not increase the FRET signals, respectively (Figure 1E). The pH dependency test demonstrated the utility of the biosensor over a wide range of pH (Figure 1F). In addition, slight pH alterations around normal cytosolic pH, which is near 7.3,[52] have small effects on the FRET signal. The initial rate of change in the FRET signal was saturated at higher BCAA concentrations, obeying Michaelis−Menten-like kinetics (Figure 1G). This suggests that the conformational changes of the biosensor consist of a very rapid BCAA-binding step, followed

DOI: 10.1021/acssensors.9b02067
ACS Sens. XXXX, XXX, XXX−XXX

Table 1. Intracellular Amino Acid Concentrations Determined by HPLC[a]

	amino acid-free DMEM				
intracellular concentration (μM)		+ 0.6 mM BCAA	+2.4 mM BCAA	DMEM	DMEM composition*
Ala	240 ± 48	218 ± 55	210 ± 22	261 ± 26	
Asn	109 ± 2	40 ± 14	38 ± 8	98 ± 15	
Asp	461 ± 10	1309 ± 19	893 ± 37	1907 ± 129	
Arg	117 ± 68	65 ± 25	81 ± 35	84 ± 2	400
Cys−Cys	nd.	nd.	nd.	21 ± 7	200
Gln	30 ± 2	nd.	32 ± 31	1663 ± 141	4000
Glu	3138 ± 222	3979 ± 118	2774 ± 73	4970 ± 90	
Gly	85 ± 27	117 ± 31	138 ± 27	1047 ± 172	400
His	28 ± 7	36 ± 8	32 ± 2	159 ± 8	200
Ile	62 ± 3	146 ± 15	549 ±64	445 ± 72	800
Leu	109 ± 31	249 ± 26	781 ± 102	615 ± 71	800
Lys	97 ± 48	104 ± 4	227 ± 5	256 ± 79	800
Met	46 ± 6	41 ± 13	59 ± 3	156 ± 22	200
Phe	54 ± 3	53 ± 19	92 ± 1	284 ± 54	400
Pro	nd.	nd.	124 ± 110	302 ± 46	
Ser	88 ± 58	37 ± 4	72 ± 34	395 ± 106	400
Thr	45 ± 13	32 ± 0	70 ± 7	806 ± 156	800
Trp	46 ± 0	32 ± 20	44 ± 2	93 ± 17	78
Tyr	49 ± 3	33 ± 0	76 ± 2	299 ± 48	400
Val	86 ± 14	181 ± 18	622 ± 75	421 ± 69	800
total	4920 ± 572	6694 ± 41	6938 ± 547	14 582 ± 560	10 678

[a]The values represent the mean ± SD (n = duplicate or triplicate). In the table, DMEM composition* and nd. represent amino acid levels in normal culture medium (DMEM) and not detected, respectively.

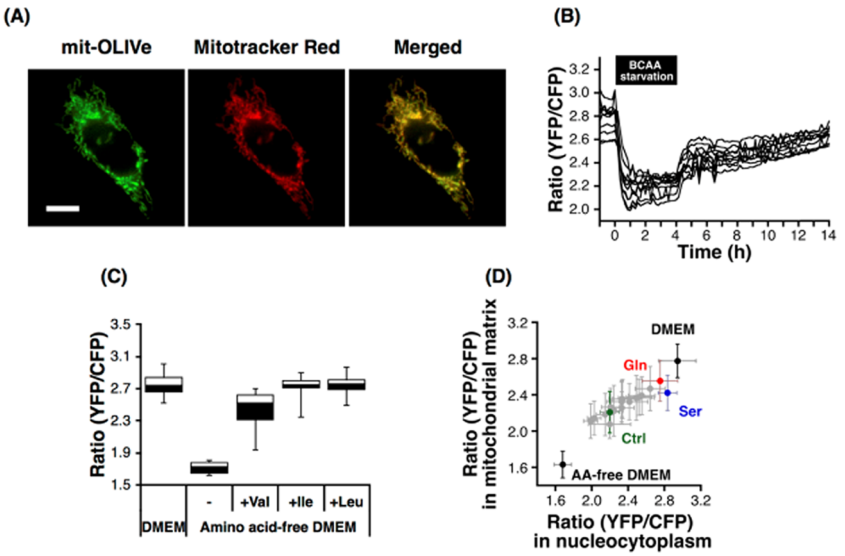

Figure 3. Visualization of BCAA levels in the mitochondrial matrix. (A) Localization of mit-OLIVe expressed in HeLa cells. Images were captured from cells labeled with 100 nM of Mitotracker Red CMXRos at 37 °C for 30 min. The panel shows fluorescence images of mit-OLIVe (left), Mitotracker Red (middle), and the merged image (right), obtained from a representative HeLa cell expressing mit-OLIVe. Scale bar represents 10 μm. (B) Representative time course of FRET signals of HeLa cells expressing mit-OLIVe. Cells were treated with DMEM without BCAAs at time = 0 and subsequently recultured in DMEM at time = 4 h. Each line represents FRET signals from individual cells. Three independent experiments gave consistent results. (C) Distribution of FRET signals of cells expressing mit-OLIVe. FRET signals were examined in cells after a 5-h treatment with amino acid-free DMEM supplemented with 1 mM of valine, isoleucine, or leucine. Box-and-whisker plots of FRET values from individual cells are shown (n = 15−36 cells for the each treatment, from two to three independent repetitions). (D) Correlation of the average FRET signals in the nucleocytoplasm and the mitochondrial matrix. FRET signals were examined 5 h after the addition of individual amino acids (1 mM) to cells preincubated in amino acid-free DMEM supplemented with 1 mM of valine for 5 h. The FRET signals from mit-OLIVe-expressing cells vs OLIVe-expressing cells were plotted in the response to each amino acid. The values represent the mean ± SD (n = 42−97 cells for each treatment, from three independent repetitions).

by a slow conformational maturation step. The apparent maximum rate was determined to be 1.8×10^{-2}, 1.7×10^{-2}, and 1.6×10^{-2} min^{-1} for leucine, isoleucine, and valine, respectively.

DOI: 10.1021/acssensors.9b02067
ACS Sens. XXXX, XXX, XXX−XXX

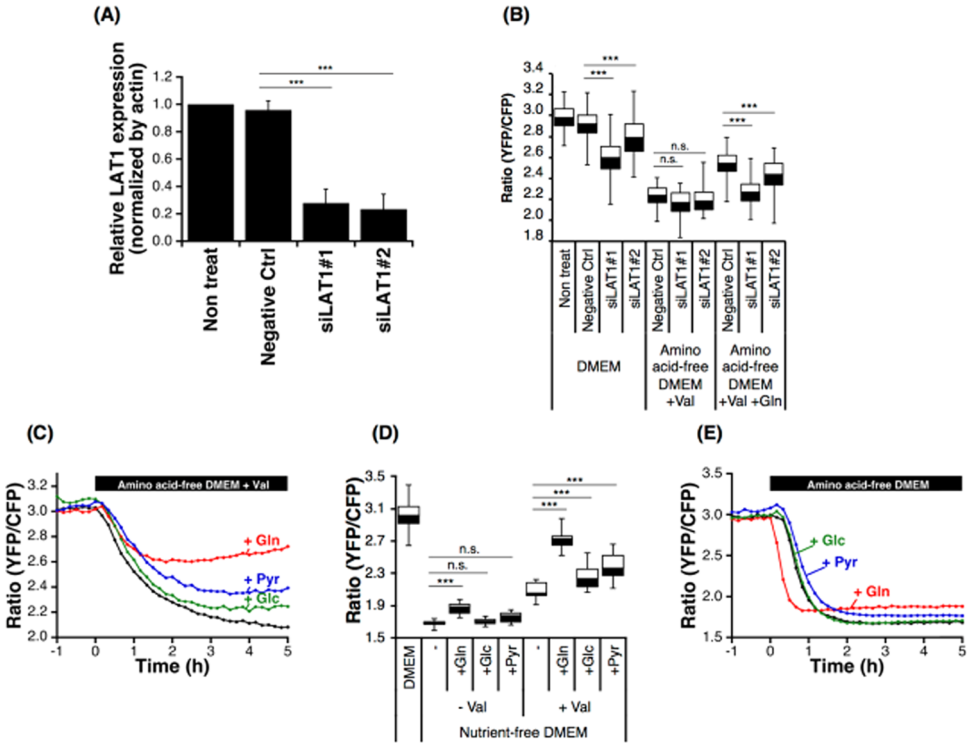

Figure 4. Impacts of extracellular nutrients on intracellular BCAA levels. (A) Expression levels of LAT1 in HeLa cells with two independent LAT1 siRNAs. (B) Effects of LAT1 knockdown on FRET signals in HeLa cells. Cells were incubated for 40 h at 37 °C in DMEM after the siRNA treatment and subjected to (A) western blot analysis (n = triplicate) or (B) the BCAA measurement using the biosensor (n = 47−130 cells, from three independent repetitions). Negative Ctrl represents cells treated with negative control siRNA. The values represent the mean ± SD. (C) Time course of average FRET signals of cells. Cells were switched to nutrient-free medium supplemented with 1 mM of valine (control, black line) and 1 g/L of glucose (green line), or 1 mM of pyruvate (blue line), or 4 mM of glutamine (red line) at time = 0 (n = 26−35 cells for each treatment, from three independent repetitions). (D) Distribution of FRET signals. Box-and-whisker plots of FRET values are shown at time = 5 h after the treatment corresponding to the assay in (C) and (E). (E) Time course of average FRET signals of cells. Cells were switched from DMEM to nutrient-free medium (control, black line) or medium containing 1 g/L of glucose (green line), or 1 mM of pyruvate (blue line), or 4 mM of glutamine (red line) at time = 0 (n = 24−33 cells for each treatment, from three independent repetitions). ***P < 0.001 by analysis of variance (ANOVA) with Tukey's post-hoc test.

Visualization of Nucleocytoplasmic BCAA Levels in Single Living Mammalian Cells. When the biosensor was expressed in cells, it localized largely in the cytosol, with a fraction in the nucleus, as examined by fluorescence (Figure 2A). FRET signals were calculated by dividing the YFP to CFP fluorescence emissions from cells upon excitation of CFP. First, we monitored the FRET signals in single cells under various culture conditions. The cells cultured in normal culture medium (DMEM) showed steady FRET signals (Figure 2B). FRET signals from cells were apparently independent of the expression levels of the biosensor in the cells, at least in our experimental condition (Figure S3). When an excess amount of BCAAs was added to the medium, FRET signals gradually increased (Figure 2B). In contrast, when the cells were cultured in amino acid starvation medium (EBSS), the FRET signals rapidly decreased and gradually recovered following the addition of BCAAs to EBSS (Figure 2C,D and Supplemental Movie 1). Recovery of the FRET signals of OLIVe from the starvation took hours (Figure 2C). This period required for the recovery may simply reflect the activity of transporters for BCAA in HeLa cells. Another possibility is that intracellular utilization of BCAA for protein synthesis and/or other metabolic pathways competes with the uptake, resulting in the slow recovery of the intracellular BCAA level.

Next, we compared the FRET signals from single OLIVe-expressing cells with bulk intracellular BCAA concentrations, which were calculated from cell populations using an HPLC technique, under various concentrations of BCAAs (Figure 2E and Table 1). As expected, bulk intracellular BCAA concentrations were highly dependent on BCAA amounts in the medium. FRET signals from the OLIVe-expressing cells were also dependent on BCAA amounts in these media and were highly correlated with the bulk intracellular BCAA concentrations (Figure 2F). The results clearly demonstrate that FRET signals from OLIVe expressed in single cells represent intracellular BCAA levels. According to the values determined by HPLC, the biosensor feasibly enabled measurements of BCAA inside cells from approximately 200 μM to 2 mM (Figure 2G).

Visualization of Mitochondrial BCAA Levels. A portion of cytosolic BCAAs should be transported into the mitochondrial matrix because BCAAs are utilized for mitochondrial protein synthesis and metabolized as cellular energy sources. However, it has been impossible to specifically monitor BCAA levels in the mitochondrial matrix. We fused two tandem copies of the mitochondrial targeting signal from cytochrome c oxidase subunit VIII to the N-terminus of OLIVe to target it to the mitochondrial matrix (Figure S1). The fused protein, mit-OLIVe, properly localized to the mitochondrial matrix, as demonstrated by its fluorescence colocalization with MitoTracker Red (Figure 3A). Similar to the result for OLIVe, we observed alterations in FRET signals from mit-OLIVe

DOI: 10.1021/acssensors.9b02067
ACS Sens. XXXX, XXX, XXX−XXX

coinciding with BCAA amounts in the culture medium (Figure 3B). Consistently, cells cultured in amino acid-free DMEM showed increased mit-OLIVe FRET signals in response to supplementation of the medium with individual BCAAs (Figure 3C). From these results, we concluded that mit-OLIVe was capable of monitoring mitochondrial BCAA levels.

Intracellular BCAA Levels are Regulated by the Nutritional Environment of the Cells. BCAA measurements using OLIVe and the HPLC technique indicated that omitting non-BCAA amino acids from DMEM apparently increased the intracellular BCAA level in cells (Figure 2E,F and Table 1), suggesting potential impacts of other amino acids on intracellular BCAA levels. To examine this, we quantified FRET signals of OLIVe-expressing cells and mit-OLIVe-expressing cells in response to the addition of individual non-BCAA amino acids to cells cultured in amino acid-free DMEM supplemented with valine (Figures 3D and S4). Interestingly, intracellular BCAA levels significantly varied depending on which amino acid was added. Of these, glutamine significantly enhanced both the nucleocytoplasmic and mitochondrial BCAA levels. We found a strong positive correlation between nucleocytoplasmic and mitochondrial BCAA levels. The results suggest that transport of BCAA from the cytoplasm to the mitochondria may largely depend on the difference of BCAA levels between the two subcellular compartments. We note that there is a large difference between the cytoplasm and the mitochondria in the case of added serine (Figures 3D and S4). This discrepancy raises the possibility that there may be distinct amino acid transport systems in the mitochondrial inner membrane as opposed to the plasma membrane in HeLa cells.

Previously, it has been reported that L-type amino acid transporter 1 (LAT1) is responsible for the large part of BCAA uptake in cancer cells, including HeLa cells.[53,54] Consistently, LAT1 knockdown cells showed significantly decreased FRET signals compared to the control cells (Figures 4A,B and S5A,B). Previous reports have suggested that glutamine influx triggers BCAA entry via the LAT1 exchanger.[55,56] Therefore, we speculated that the observed glutamine-mediated increase in intracellular BCAA levels was achieved through LAT1 activity. As expected, we observed that LAT1 knockdown significantly suppressed the increase in FRET signals by addition of glutamine (Figure 4B). These results clearly demonstrated that LAT1 is a key transporter determining intracellular BCAA levels in HeLa cells.

BCAAs are potent nutritional signaling molecules that regulate cellular metabolic processes, such as glucose and protein synthesis.[2] Therefore, utilization of BCAAs may be regulated according to the availability of cellular energy sources in the environment to maintain cellular homeostasis. Based on this notion, we further characterized the impacts of glutamine as well as glucose and pyruvate on intracellular BCAA levels by time-lapse BCAA imaging. HeLa cells cultured in nutrient-free medium supplemented with valine gradually lost nucleocytoplasmic BCAAs over time (Figure 4C). On the other hand, we observed significantly maintained BCAA levels in the presence of glutamine (Figure 4C,D), consistent with the above results (Figure 3D). Interestingly, cells retained slightly higher BCAA levels in the presence of glucose or pyruvate during starvation compared to control cells. This observation suggests that not only glutamine but also glucose and pyruvate enhance uptake of BCAAs into the cells since HeLa cells are unable to synthesize BCAAs. Supporting this idea, the nutrient-mediated increases in BCAA levels were not observed in the absence of valine (Figure 4E). Although the addition of glucose or pyruvate may affect intracellular pH, effects of pH on the observed FRET increases upon adding glucose or pyruvate (Figure 4C) must be negligible because the FRET increases were not observed in the absence of valine (Figure 4E). However, care must be taken in interpreting the FRET signals of OLIVe under particular conditions where large pH changes occur, for example in glucose-starved yeast cells,[57] because OLIVe's signal could be altered at a relatively high or low pH (Figure 1F) and fluorescent proteins can be more sensitive to pH in vivo than in vitro.[58]

Our results indicate that intracellular BCAA levels are determined not only by environmental BCAA levels and transporter activity but also by other nutrients in the environment. Imaging of intracellular BCAA levels with the fluorescent biosensor will be a key technique to understand this complex behavior of BCAAs inside cells.

CONCLUSIONS

To monitor intracellular BCAA concentrations in space and time, we developed a genetically encoded FRET biosensor for BCAAs, termed OLIVe. The relatively large (≈100%) FRET gain of OLIVe suggests that the insertion of a donor and/or an acceptor fluorescent protein within a sensory protein could be a viable alternative strategy to the more typical addition of the fluorescent proteins to the termini. This strategy can be especially effective when the distance between the termini is almost unchanged upon ligand binding, but internal conformational changes are larger. The FRET signal of the purified OLIVe increased in response to each BCAA species, leucine, isoleucine, and valine. Although it also responds slightly to high concentrations of cysteine, threonine, and methionine, the effect of these amino acids can be ignored when using OLIVe in cultured mammalian cells because the intracellular concentrations of these amino acids are below 1 mM in normal culture conditions (Table 1). Although OLIVe was functional over a wide range of pH, we did observe some pH-dependent changes in the FRET signal. Thus, large alterations of pH should be avoided when comparing OLIVe signals in different conditions. The FRET signal of intracellularly expressed OLIVe was highly dependent on the medium BCAA level, and was highly correlated with biochemically determined intracellular BCAA concentrations, confirming that OLIVe also functions inside mammalian cells. Surprisingly, we found that the presence of non-BCAA amino acids, as well as glucose and pyruvate, significantly affected the intracellular BCAA concentration. Although the mechanism governing how these metabolites change intracellular BCAA levels is unknown, our results indicate that the intracellular BCAA concentration is determined by a complex context of the nutritional environment of the cell. Finally, we showed that knockdown of the LAT1 amino acid transporter significantly decreased the basal BCAA level and also abolished the glutamine-induced BCAA increase. Recent preclinical studies and drug developments for cancer have been exploiting the potential of amino acid transporters as therapeutic targets, including LAT1.[59] Therefore, BCAA imaging might be applied to screen anticancer drugs that inhibit transporters impacting BCAAs in cancer cells.

DOI: 10.1021/acssensors.9b02067
ACS Sens. XXXX, XXX, XXX−XXX

■ ASSOCIATED CONTENT

Supporting Information

The Supporting Information is available free of charge at https://pubs.acs.org/doi/10.1021/acssensors.9b02067.

Structures and sequences for OLIVe; effects of redox states on FRET signals of OLIVe; relationship of expression level of OLIVe and FRET ratio; comparison of FRET signals in the nucleocytoplasm and the mitochondrial matrix; contribution of LAT1 to intracellular BCAA levels (Figures S1−S5) (PDF)

FRET imaging video of intracellular BCAA levels in a live HeLa cell2 (Supplemental Movie 1) (AVI)

■ AUTHOR INFORMATION

Corresponding Author

*E-mail: imamura@lif.kyoto-u.ac.jp.

ORCID

Hiromi Imamura: 0000-0002-1896-0443

Author Contributions

T.Y. and H.I. conceived and designed the study. T.Y., H.N., and S.T. performed the experiments. T.Y., H.N., and H.I. analyzed the results. T.Y., A.K., and H.I. wrote the manuscript.

Notes

The authors declare no competing financial interest.

■ ACKNOWLEDGMENTS

We thank James Alan Hejna, Kunio Takeyasu, and Promise Ogor for critical assessment of this manuscript. This work was supported by JSPS KAKENHI Grant Number 17H03654 and by a grant from the Nakatani Foundation (to H.I.).

■ ABBREVIATIONS

BCAA, branched-chain amino acid; FRET, Förster resonance energy transfer; CFP, cyan fluorescent protein; YFP, yellow fluorescent protein; DMEM, Dulbecco's modified Eagle's medium

■ REFERENCES

(1) Brosnan, J. T.; Brosnan, M. E. Branched-chain amino acids: enzyme and substrate regulation. *J. Nutr.* **2006**, *136*, 207S−211S.

(2) Nie, C.; He, T.; Zhang, W.; Zhang, G.; Ma, X. Branched chain amino acids: Beyond nutrition metabolism. *Int. J. Mol. Sci.* **2018**, *19*, No. 954.

(3) Kawaguchi, T.; Izumi, N.; Charlton, M. R.; Sata, M. Branched-chain amino acids as pharmacological nutrients in chronic liver disease. *Hepatology* **2011**, *54*, 1063−1070.

(4) Holecek, M. Three targets of branched-chain amino acid supplementation in the treatment of liver disease. *Nutrition* **2010**, *26*, 482−490.

(5) Kopple, J. D.; Kalantar-Zadeh, K.; Mehrotra, R. Risks of chronic metabolic acidosis in patients with chronic kidney disease. *Kidney Int.* **2005**, *67*, S21−S27.

(6) Kumar, M. A.; Bitla, A. R.; Raju, K. V.; Manohar, S. M.; Kumar, V. S.; Narasimha, S. R. Branched chain amino acid profile in early chronic kidney disease. *Saudi J. Kidney Dis. Transpl.* **2012**, *23*, 1202−1207.

(7) Schols, A. M. Nutritional and metabolic modulation in chronic obstructive pulmonary disease management. *Eur. Respir. J.* **2003**, *22*, 81s−86s.

(8) Rodney, S.; Boneh, A. Amino Acid Profiles in Patients with Urea Cycle Disorders at Admission to Hospital due to Metabolic Decompensation. *JIMD Rep.* **2013**, *9*, 97−104.

(9) Jeter, C. B.; Hergenroeder, G. W.; Ward, N. H., 3rd; Moore, A. N.; Dash, P. K. Human Mild Traumatic Brain Injury Decreases Circulating Branched-Chain Amino Acids and Their Metabolite Levels. *J. Neurotrauma* **2013**, *30*, 671−679.

(10) Yoon, M. S. The Emerging Role of Branched-Chain Amino Acids in Insulin Resistance and Metabolism. *Nutrients* **2016**, *8*, No. 405.

(11) Suhre, K.; Meisinger, C.; Döring, A.; Altmaier, E.; Belcredi, P.; Gieger, C.; Chang, D.; Milburn, M. V.; Gall, W. E.; Weinberger, K. M.; Mewes, H. W.; Hrabé de Angelis, M.; Wichmann, H. E.; Kronenberg, F.; Adamski, J.; Illig, T. Metabolic Footprint of Diabetes: A Multiplatform Metabolomics Study in an Epidemiological Setting. *PLoS One* **2010**, *5*, No. e13953.

(12) Wolak-Dinsmore, J.; Gruppen, E. G.; Shalaurova, I.; Matyus, S. P.; Grant, R. P.; Gegen, R.; Bakker, S. J. L.; Otvos, J. D.; Connelly, M. A.; Dullaart, R. P. F. A novel NMR-based assay to measure circulating concentrations of branched-chain amino acids: Elevation in subjects with type 2 diabetes mellitus and association with carotid intima media thickness. *Clin. Biochem.* **2018**, *54*, 92−99.

(13) Bhattacharya, S.; Granger, C. B.; Craig, D.; Haynes, C.; Bain, J.; Stevens, R. D.; Hauser, E. R.; Newgard, C. B.; Kraus, W. E.; Newby, L. K.; Shah, S. H. Validation of the association between a branched chain amino acid metabolite profile and extremes of coronary artery disease in patients referred for cardiac catheterization. *Atherosclerosis* **2013**, *232*, 191−196.

(14) Ruiz-Canela, M.; Toledo, E.; Clish, C. B.; Hruby, A.; Liang, L.; Salas-Salvadó, J.; Razquin, C.; Corella, D.; Estruch, R.; Ros, E.; Fitó, M.; Gómez-Gracia, E.; Arós, F.; Fiol, M.; Lapetra, J.; Serra-Majem, L.; Martínez-González, M. A.; Hu, F. B. Plasma Branched-Chain Amino Acids and Incident Cardiovascular Disease in the PREDIMED Trial. *Clin. Chem.* **2016**, *62*, 582−592.

(15) Morton, D. H.; Strauss, K. A.; Robinson, D. L.; Puffenberger, E. G.; Kelley, R. I. Diagnosis and Treatment of Maple Syrup Disease: A Study of 36 Patients. *Pediatrics* **2002**, *109*, 999−1008.

(16) She, P.; Van Horn, C.; Reid, T.; Hutson, S. M.; Cooney, R. N.; Lynch, C. J. Obesity-related elevations in plasma leucine are associated with alterations in enzymes involved in branched chain amino acid (BCAA) metabolism. *Am. J. Physiol.: Endocrinol. Metab.* **2007**, *293*, E1552−E1563.

(17) Charlton, M. Branched-Chain Amino Acid Enriched Supplements as Therapy for Liver Disease. *J. Nutr.* **2006**, *136*, 295S−298S.

(18) Cole, J. T.; Mitala, C. M.; Kundu, S.; Verma, A.; Elkind, J. A.; Nissim, I.; Cohen, A. S. Dietary branched chain amino acids ameliorate injury-induced cognitive impairment. *Proc. Natl. Acad. Sci. U.S.A.* **2010**, *107*, 366−371.

(19) Elkind, J. A.; Lim, M. M.; Johnson, B. N.; Palmer, C. P.; Putnam, B. J.; Kirschen, M. P.; Cohen, A. S. Efficacy, Dosage, and Duration of Action of Branched Chain Amino Acid Therapy for Traumatic Brain Injury. *Front. Neurol.* **2015**, *6*, No. 73.

(20) Fontana, L.; Cummings, N. E.; Arriola Apelo, S. I.; Neuman, J. C.; Kasza, I.; Schmidt, B. A.; Cava, E.; Spelta, F.; Tosti, V.; Syed, F. A.; Baar, E. L.; Veronese, N.; Cottrell, S. E.; Fenske, R. J.; Bertozzi, B.; Brar, H. K.; Pietka, T.; Bullock, A. D.; Figenshau, R. S.; Andriole, G. L.; Merrins, M. J.; Alexander, C. M.; Kimple, M. E.; Lamming, D. W. Decreased Consumption of Branched-Chain Amino Acids Improves Metabolic Health. *Cell Rep.* **2016**, *16*, 520−530.

(21) Pedroso, J. A.; Zampieri, T. T.; Donato, J., Jr. Reviewing the Effects of L-Leucine Supplementation in the Regulation of Food Intake, Energy Balance, and Glucose Homeostasis. *Nutrients* **2015**, *7*, 3914−3937.

(22) Hasegawa, T.; Ikeda, H. O.; Iwai, S.; Muraoka, Y.; Tsuruyama, T.; Okamoto, K. F.; Kohda, H.; Kakizuka, A.; Yoshimura, N. Branched chain amino acids attenuate major pathologies in mouse models of retinal degeneration and glaucoma. *Heliyon* **2018**, *4*, No. e00544.

(23) Mattick, J. S. A.; Kamisoglu, K.; Ierapetritou, M. G.; Androulakis, I. P.; Berthiaume, F. Branched-chain amino acid supplementation: impact on signaling and relevance to critical illness. *Wiley Interdiscip. Rev.: Syst. Biol. Med.* **2013**, *5*, 449−460.

DOI: 10.1021/acssensors.9b02067
ACS Sens. XXXX, XXX, XXX−XXX

(24) D'Antona, G.; Ragni, M.; Cardile, A.; Tedesco, L.; Dossena, M.; Bruttini, F.; Caliaro, F.; Corsetti, G.; Bottinelli, R.; Carruba, M. O.; Valerio, A.; Nisoli, E. Branched-Chain Amino Acid Supplementation Promotes Survival and Supports Cardiac and Skeletal Muscle Mitochondrial Biogenesis in Middle-Aged Mice. *Cell Metab.* **2010**, *12*, 362−372.
(25) Juricic, P.; Grönke, S.; Partridge, L. Branched-Chain Amino Acids Have Equivalent Effects to Other Essential Amino Acids on Lifespan and Aging-Related Traits in Drosophila. *J. Gerontol., Ser. A* **2019**, No. glz080.
(26) Mansfeld, J.; Urban, N.; Priebe, S.; Groth, M.; Frahm, C.; Hartmann, N.; Gebauer, J.; Ravichandran, M.; Dommaschk, A.; Schmeisser, S.; Kuhlow, D.; Monajembashi, S.; Bremer-Streck, S.; Hemmerich, P.; Kiehntopf, M.; Zamboni, N.; Englert, C.; Guthke, R.; Kaleta, C.; Platzer, M.; Sühnel, J.; Witte, O. W.; Zarse, K.; Ristow, M. Branched-chain amino acid catabolism is a conserved regulator of physiological ageing. *Nat. Commun.* **2015**, *6*, No. 10043.
(27) Azuma, Y.; Maekawa, M.; Kuwabara, Y.; Nakajima, T.; Taniguchi, K.; Kanno, T. Determination of branched-chain amino acids and tyrosine in serum of patients with various hepatic diseases, and its clinical usefulness. *Clin. Chem.* **1989**, *35*, 1399−1403.
(28) Spackman, D. H.; Stein, W. H.; Moore, S. Automatic recording apparatus for use in chromatography of amino acids. *Anal. Chem.* **1958**, *30*, 1190−1206.
(29) Bayer, E.; Grom, E.; Kalteneger, B.; Uhmann, R. Separation of amino acids by high performance liquid chromatography. *Anal. Chem.* **1976**, *48*, 1106−1109.
(30) Zlatkis, A. J. F.; Oro, J. F.; Kimball, A. P. Direct amino acid analysis by gas chromatography. *Anal. Chem.* **1960**, *32*, 162−164.
(31) Tao, L.; Thompson, J. E.; Kennedy, R. T. Optically gated capillary electrophoresis of o-phthalaldehyde/β-mercaptoethanol derivatives of amino acids for chemical monitoring. *Anal. Chem.* **1998**, *70*, 4015−4022.
(32) Pietzsch, J.; Julius, U.; Hanefeld, M. Stable isotope ratio analysis of amino acids: the use of N(O,S)-ethoxycarbonyl trifluoroethyl ester derivatives and gas chromatography/mass spectrometry. *Rapid Commun. Mass Spectrom.* **1997**, *11*, 1835−1838.
(33) Van Leuken, R. G. J.; Duchateau, A. L. L.; Kwakkenbos, G. T. C. Thermospray liquid chromatography/mass spectrometry study of diastereomeric isoindole derivatives of amino acids and amino acid amides. *J. Pharm. Biomed. Anal.* **1995**, *13*, 1459−1464.
(34) Casetta, B.; Tagliacozzi, D.; Shushan, B.; Federici, G. Development of a method for rapid quantitation of amino acids by liquid chromatography-tandem mass spectrometry (LC-MSMS) in plasma. *Clin. Chem. Lab. Med.* **2000**, *38*, 391−401.
(35) Fehr, M.; Lalonde, S.; Lager, I.; Wolff, M. W.; Frommer, W. B. In vivo imaging of the dynamics of glucose uptake in the cytosol of COS-7 cells by fluorescentnanosensors. *J. Biol. Chem.* **2003**, *278*, 19127−19133.
(36) Okumoto, S.; Looger, L. L.; Micheva, K. D.; Reimer, R. J.; Smith, S. J.; Frommer, W. B. Detection of glutamate release from neurons by genetically encoded surface-displayed FRET nanosensors. *Proc. Natl. Acad. Sci. U.S.A.* **2005**, *102*, 8740−8745.
(37) Imamura, H.; Nhat, K. P.; Togawa, H.; Saito, K.; Iino, R.; Kato-Yamada, Y.; Nagai, T.; Noji, H. Visualization of ATP levels inside single living cells with fluorescence resonance energy transfer-based genetically encoded indicators. *Proc. Natl. Acad. Sci. U.S.A.* **2009**, *106*, 15651−15656.
(38) Hung, Y. P.; Albeck, J. G.; Tantama, M.; Yellen, G. Imaging cytosolic NADH-NAD(+) redox state with a genetically encoded fluorescent biosensor. *Cell Metab.* **2011**, *14*, 545−554.
(39) Zhao, Y.; Jin, J.; Hu, Q.; Zhou, H. M.; Yi, J.; Yu, Z.; Xu, L.; Wang, X.; Yang, Y.; Loscalzo, J. Genetically encoded fluorescent sensors for intracellular NADH detection. *Cell Metab.* **2011**, *14*, 555−566.
(40) Yoshida, T.; Alfaqaan, S.; Sasaoka, N.; Imamura, H. Application of FRET-based biosensor "ATeam" for visualization of ATP levels in the mitochondrial matrix of living mammalian cells. *Methods Mol. Biol.* **2017**, *1567*, 231−243.
(41) Yoshida, T.; Kakizuka, A.; Imamura, H. BTeam, a novel BRET-based biosensor for the accurate quantification of ATP concentration within living cells. *Sci. Rep.* **2016**, *6*, No. 39618.
(42) Saper, M. A.; Quiocho, F. A. Leucine, isoleucine, valine-binding protein from *Escherichia coli*. Structure at 3.0-A resolution and location of the binding site. *J. Biol. Chem.* **1983**, *258*, 11057−11062.
(43) Hwang, C.; Sinskey, A. J.; Lodish, H. F. Oxidized redox state of glutathione in the endoplasmic reticulum. *Science* **1992**, *257*, 1496−1502.
(44) Matsuda, T.; Miyawaki, A.; Nagai, T. Direct measurement of protein dynamics inside cells using a rationally designed photo-convertible protein. *Nat. Methods* **2008**, *5*, 339−345.
(45) Nagai, T.; Yamada, S.; Tominaga, T.; Ichikawa, M.; Miyawaki, A. Expanded dynamic range of fluorescent indicators for Ca^{2+} by circularly permuted yellow fluorescent proteins. *Proc. Natl. Acad. Sci. U.S.A.* **2004**, *101*, 10554−10559.
(46) Dwyer, M. A.; Hellinga, H. W. Periplasmic binding proteins: a versatile superfamily for protein engineering. *Curr. Opin. Struct. Biol.* **2004**, *14*, 495−504.
(47) Berntsson, R. P.; Smits, S. H.; Schmitt, L.; Slotboom, D. J.; Poolman, B. A structural classification of substrate-binding proteins. *FEBS Lett.* **2010**, *584*, 2606−2617.
(48) Fehr, M.; Frommer, W. B.; Lalonde, S. Visualization of maltose uptake in living yeast cells by fluorescent nanosensors. *Proc. Natl. Acad. Sci. U.S.A.* **2002**, *99*, 9846−9851.
(49) Trakhanov, S.; Vyas, N. K.; Luecke, H.; Kristensen, D. M.; Ma, J.; Quiocho, F. A. Ligand-free and-bound structures of the binding protein (LivJ) of the Escherichia coli ABC leucine/isoleucine/valine transport system: trajectory and dynamics of the interdomain rotation and ligand specificity. *Biochemistry* **2005**, *44*, 6597−6608.
(50) Mohsin, M.; Abdin, M. Z.; Nischal, L.; Kardam, H.; Ahmad, A. Genetically encoded FRET-based nanosensor for in vivo measurement of leucine. *Biosens. Bioelectron.* **2013**, *50*, 72−77.
(51) Kaper, T.; Looger, L. L.; Takanaga, H.; Platten, M.; Steinman, L.; Frommer, W. B. Nanosensor detection of an immunoregulatory tryptophan influx/kynurenine efflux cycle. *PLoS Biol.* **2007**, *5*, No. e257.
(52) Llopis, J.; McCaffery, J. M.; Miyawaki, A.; Farquhar, M. G.; Tsien, R. Y. Measurement of cytosolic, mitochondrial, and Golgi pH in single living cells with green fluorescent proteins. *Proc. Natl. Acad. Sci. U.S.A.* **1998**, *95*, 6803−6808.
(53) Ganapathy, V.; Thangaraju, M.; Prasad, P. D. Nutrient transporters in cancer: relevance to warburg hypothesis and beyond. *Pharmacol. Ther.* **2009**, *121*, 29−40.
(54) Yanagida, O.; Kanai, Y.; Chairoungdua, A.; Kim, D. K.; Segawa, H.; Nii, T.; Cha, S. H.; Matsuo, H.; Fukushima, J.; Fukasawa, Y.; Tani, Y.; Taketani, Y.; Uchino, H.; Kim, J. Y.; Inatomi, J.; Okayasu, I.; Miyamoto, K.; Takeda, E.; Goya, T.; Endou, H. Human L-type amino acid transporter 1 (LAT1): characterization of function and expression in tumor cell lines. *Biochim. Biophys. Acta* **2001**, *1514*, 291−302.
(55) Cluntun, A. A.; Luckey, J. M.; Cerione, A. R.; Locasale, W. J. Glutamine metabolism in cancer therapy. *Trends Cancer* **2018**, *3*, 169−180.
(56) Nicklin, P.; Bergman, P.; Zhang, B.; Triantafellow, E.; Wang, H.; Nyfeler, B.; Yang, H.; Hild, M.; Kung, C.; Wilson, C.; Myer, V. E.; MacKeigan, J. P.; Porter, J. A.; Wang, Y. K.; Cantley, L. C.; Finan, P. M.; Murphy, L. O. Bidirectional Transport of Amino Acids Regulates mTOR and Autophagy. *Cell* **2009**, *136*, 521−534.
(57) Munder, M. C.; Midtvedt, D.; Franzmann, T.; Nüske, E.; Otto, O.; Herbig, M.; Ulbricht, E.; Müller, P.; Taubenberger, A.; Maharana, S.; Malinovska, L.; Richter, D.; Guck, J.; Zaburdaev, V.; Alberti, S. A pH-driven transition of the cytoplasm from a fluid- to a solid-like state promotes entry into dormancy. *Elife* **2016**, *5*, No. e09347.
(58) Botman, D.; Groot, D. H.; Schmidt, P.; Goedhart, J.; Teusink, B. In vivo characterisation of fluorescent proteins in budding yeast. *Sci. Rep.* **2019**, *9*, No. 2234.
(59) Bhutia, Y. D.; Babu, E.; Ramachandran, S.; Ganapathy, V. Amino Acid Transporters in Cancer and Their Relevance to

DOI: 10.1021/acssensors.9b02067
ACS Sens. XXXX, XXX, XXX−XXX

"Glutamine Addiction": Novel Targets for the Design of a New Class of Anticancer Drugs. *Cancer Res.* **2015**, *75*, 1782−1788.

DOI: 10.1021/acssensors.9b02067
ACS Sens. XXXX, XXX, XXX−XXX